ELSEVIER

Journal of Hydrology 203 (1997) 58–78

Journal of Hydrology

Analysis of focused unsaturated flow beneath fissures in the Chihuahuan Desert, Texas, USA

Bridget R. Scanlon*, Richard S. Goldsmith, Jeffrey G. Paine

Bureau of Economic Geology, The University of Texas at Austin, Austin, TX 78713-8924, USA

Received 26 November 1996; revised 20 June 1997; accepted 20 June 1997

Abstract

Localized flow beneath fissures in arid settings has important implications for waste disposal in these regions. Fissures are surface features or gullies that are underlain by sediment filled fractures. The objectives of this study were to compare unsaturated flow beneath different fissures, investigate the vertical and lateral extent of increased flow associated with fissures, and examine different techniques for evaluating flow in zones containing fissures. Boreholes were drilled directly beneath four fissures and at horizontal distances of 10 and 50 m from the fissures. Physical parameters such as water content and water potential were analyzed in sediment samples and water potential was analyzed in plant samples. Environmental tracers such as Cl, $^{36}Cl/Cl$, ^{3}H, D, and ^{18}O were analyzed in sediment samples. A trench was dug beneath one fissure for detailed sampling. Electromagnetic induction was used to measure apparent electrical conductivity in transects perpendicular to the fissures.

Unsaturated flow is relatively higher beneath fissures, as evidenced by higher water potentials and lower chloride concentrations there than in surrounding sediments. The lateral extent of high water flux was restricted to the zone directly beneath one fissure but extended to profiles 10 m from two other fissures. The profiles 50 m from all fissures had low water fluxes, as indicated by low water potentials and high maximum chloride concentrations. The vertical extent of high water fluxes was restricted to the upper 10 to 20 m zone, as shown by water potential and chloride fronts within the upper 10 m zone beneath one fissure and by chloride fronts in the upper 20 m zone beneath and 10 m from another fissure. Additional evidence for localized water flux was provided by less enriched D and ^{18}O, and higher plant water potentials in sediments beneath fissures relative to sediments adjacent to fissures. High tritium levels were found in all sampled profiles and cannot readily be explained. Apparent electrical conductivity was higher in two of the four fissures. Multiple independent lines of evidence indicate that subsurface water fluxes are higher at shallow depths beneath fissures; however, the various techniques differ in their effectiveness in delineating higher water fluxes beneath fissures. Multiple profiles drilled in one fissure indicate that there is large variability in flow along this fissure that is attributed to topographic variations and degree of ponding. © 1997 Elsevier Science B.V.

Keywords: Unsaturated zone; Fissures; Electromagnetic induction; Chlorides

1. Introduction

Surface fissures have been found in semiarid and arid regions throughout the western United States from southern California to western Texas and as far north as Idaho (Baumgardner and Scanlon, 1992). Linear systems of fissures are as much as 15 km

* Corresponding author at: The University of Texas at Austin, Bureau of Economic Geology, 10100 Burnet Road, Bldg 130, Austin, TX 78713 4497, USA. e-mail: scanlonb@begv.begutexas.edu

PII S0022-1694(97)00086-3

long (Slaff, 1989). Individual fissures as wide as 15 m and fractures as deep as 25 m have been found (Boling, 1986; Slaff, 1989).

The term *fissure* refers to the alignment of discontinuous surface collapse structures, or gullies; the underlying extensional feature, termed a *fracture*, is filled with sediment. Fissures commonly form in sediments near margins of alluvial valleys. They are generally oriented parallel or subparallel to the long axis of the host valley and approximately perpendicular to tributary drainage. Because of their orientation they intercept runoff, which erodes the fissures into wide gullies. The increased runoff into fissures results in higher water content and vegetation being concentrated in these zones.

Many fissures have formed where sediment compaction and land subsidence have resulted from groundwater withdrawal, particularly in Arizona (Schumann et al., 1986). However, some fissures have formed in areas where groundwater pumping has been minimal or before extensive groundwater pumping began (Robinson and Peterson, 1962; Slaff, 1989). Baumgardner and Scanlon (1992) suggested that the model for fissure development proposed by Larson and Péwé (1986) should be applicable to fissures in the study area. According to this model, the initial feature is a fracture that forms in the shallow subsurface and allows water to move down from the surface. Water movement leads to erosion of the fracture and creates horizontal soil pipes. Eventually the sediments overlying the pipes collapse, which results in surface gullies that concentrate runoff. The gullies eventually connect, and the final phase is marked by plugging of the soil pipes and filling of the fissure with sediment.

The objectives of this study were to compare unsaturated flow beneath different fissures, to determine the vertical and lateral extent of increased flow beneath fissures, and to evaluate different techniques of estimating unsaturated flow beneath fissures. Fissures evaluated in this study included the Hueco Bolson fissure that was previously studied (Scanlon, 1992b) and three additional fissures (Eagle Flat, Red Light Bolson, and Ryan Flat). This study examined the vertical extent of unsaturated flow by drilling and sampling boreholes to a maximum depth of 31 m, whereas in the previous investigation of the Hueco Bolson fissure the maximum borehole depth was 9 m. To evaluate the lateral extent of increased flow associated with fissures, boreholes for this study were drilled at distances of 10 and 50 m from each fissure, whereas the previous study only included boreholes at distances of 3 and 6 m. A large trench was excavated beneath one fissure for detailed sampling. In this study, the number of techniques used to evaluate unsaturated flow beneath fissures was greatly increased from those used in the previous study (Scanlon, 1992b). In the previous study, chloride was the only environmental tracer used, whereas chloride, chlorine-36, tritium, and stable isotopes of oxygen and hydrogen were also used in this study. The use of noninvasive techniques such as electromagnetic induction and plant water potentials was also evaluated in this study. The following provides a brief description of the theoretical basis for the various techniques used.

Physical data included water content and water potential measured on sediment samples collected from boreholes drilled in and adjacent to the fissures. Water content is discontinuous across different sediment types; therefore, variations in water content measured at one time cannot be used to evaluate the direction of water movement. In contrast, water potential is continuous across different textural interfaces under steady flow conditions, and water potential gradients can be used to assess the direction of water movement. Predawn plant water potentials are generally considered to give an indication of the water potential in unsaturated sediments and should provide a noninvasive technique of estimating unsaturated flow. Previous studies showed that water potentials in the unsaturated zone were much higher in sediments beneath fissures than in sediments adjacent to fissures (Scanlon, 1992b); therefore, predawn plant water potentials in zones beneath fissures should be higher than those in zones adjacent to fissures. Electromagnetic induction provides a noninvasive technique for evaluating apparent electrical conductivity of the sediments. Fractures and soil pipes with associated high water flux may exist in the subsurface for a long time with little surface expression; therefore, noninvasive techniques may be particularly useful for delineating these zones prior to surface collapse and gully formation.

Environmental tracers are being used extensively to quantify water fluxes in the unsaturated zone. Chloride

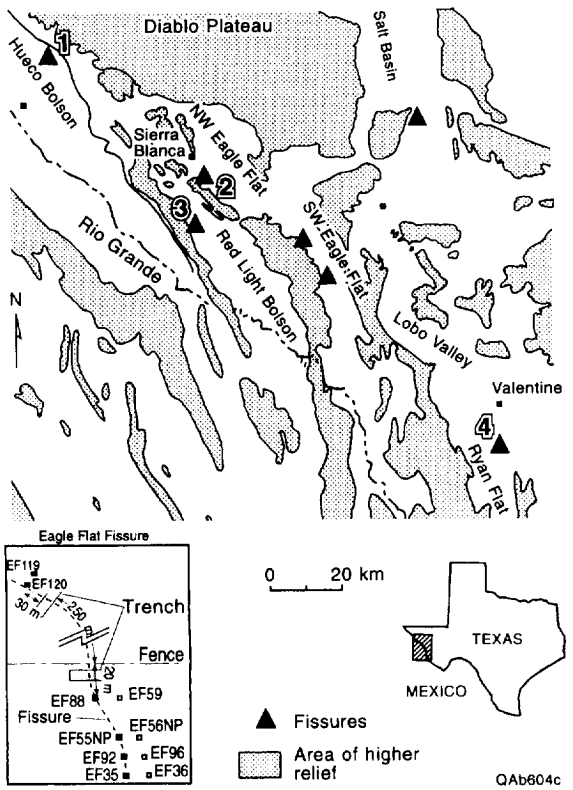

Fig. 1. Location of fissures (modified from Baumgardner and Scanlon, 1992).

concentrations in pore water have been widely used to evaluate water fluxes in arid and semiarid systems (Allison and Hughes, 1978Edmunds and Walton, 1980; Phillips, 1994). Chloride concentrations in pore water in the unsaturated zone increase through the root zone as a result of evapotranspiration because chloride is essentially nonvolatile and plant uptake is negligible. Low chloride concentrations reflect high water fluxes that either minimize accumulation of chloride or flush out previously accumulated chloride. High chloride concentrations indicate low water flux because chloride accumulates as a result of evapotranspiration.

The subsurface distribution of bomb pulse tracers such as chlorine-36 and tritium provides information on water movement during the past 30 to 40 years. Chlorine-36 (half-life 301 000 yr) was enriched by neutron activation of chlorine-35 in sea water by nuclear weapons tests conducted between 1952 and 1958, and chlorine-36 production peaked in 1955 (Bentley et al., 1986). Chlorine-36 production as a result of weapons testing exceeded natural production by up to three orders of magnitude (Bentley et al., 1986). Tritium (half-life 12.4 yr) concentrations increased from 10 to ≥2000 tritium units (TU) during atmospheric nuclear testing that began in 1952 and peaked in 1963 to 1964.

1.1. Site description

Fissures examined in this study are located in intermontane basins within the Basin and Range physiographic province in Trans-Pecos Texas (Fig. 1). Studies were conducted in the Hueco Bolson, Red Light Bolson, Eagle Flat, and Ryan Flat fissures. The Hueco Bolson site was originally considered for low level radioactive waste disposal. Fissures at the Eagle Flat site are northwest of the current proposed site for low level radioactive waste disposal. The other fissures were chosen because they provide examples of different types of fissures in the region (Red Light Bolson, mature; Ryan Flat, young). All fissures are found in alluvial fill sediments. Depth to groundwater ranges from 85 m (Ryan Flat fissure) to 215 m (Eagle Flat fissure).

Three of the four studied fissures are described in detail in Baumgardner and Scanlon (1992), and the fourth fissure (Eagle Flat) is described in Jackson et al. (1993); therefore, only brief descriptions are provided here. Width-to-depth (width/depth) ratios of surface gullies of fissures provide some indication of the maturity of the fissures and range from 0.1 to 28; however, most are ≤5. Very low width/depth ratios are indicative of young fissures, whereas those with high width/depth ratios are probably filling and widening and are relatively mature.

Three fissures were mapped in the Hueco Bolson and ranged from 21 to 140 m long. These fissures are in fairly coarse textured sediments. Studies were conducted in the 140 m long fissure, which had width/depth ratios that ranged from 0.2 to 2. This fissure is marked by honey mesquite trees (*Prosopis glandulosa*). The surface collapse features are separated by bridges of sediment that overlie soil pipes. Spacing between collapsed sections is generally 1 to 3 m. Trenches revealed subsurface fractures that extend to a depth of at least 6.2 m. The fracture width ranges

Fig. 2. View of Eagle Flat fissure on aerial photograph taken in 1991.

from 65 mm at 3.8 m depth to 25 mm at 5.6 m depth and is filled with sediment. The fissure is not visible on aerial photographs because of large creosote bushes (*Larrea tridentata*) adjacent to the fissures.

The fissure studied in Red Light Bolson lies at the toe of a dissected alluvial fan. The fissure trends 10°N–25°W, parallel to topographic contours and to the valley axis. Fissures in this area were up to 4.2 km long on aerial photographs taken in 1957. The northwest-trending fissures are perpendicular to the ephemeral stream channels and intercept runoff. Mesquite trees are denser in the vicinity of the fissure. These fissures have filled with sediment and have width/depth ratios up to 5. Another section of the Red Light Bolson fissures showed evidence of recent collapse and had steep gullies (3.6 m deep and 0.8 m wide). Calcic soil development is much greater in this section of the fissure and maintains the open gullies.

The northwest Eagle Flat fissure is 640 m long and is clearly delineated on aerial photographs taken in 1991 (Fig. 2) and on the ground by mesquite trees. It consists of depressions that average 20 m long, 1 m wide, and 0.3 m deep. Trenches dug to a maximum depth of 6 m showed a modern calcic soil and three buried calcic soils (Fig. 3). The fissure or gully is underlain by a tension fracture that is most obvious at depths of 2 m or more. At shallower depths, the fracture is not as obvious because of slumping of sediments. The width of the eroded fracture is ~0.2 m in the depth zone from 2 to 6 m. At ~3.5 m depth the fracture bifurcates, and one of the bifurcations is only 0.04 m wide. The maximum vertical extent of the fracture is unknown because the trench did not reach the base of the fracture. The fracture fill sediments are slightly coarser grained than the surrounding material. The fissure formed as a result of near-surface tensional stresses.

Gullies associated with the fissures in Ryan Flat opened at the surface in 1990. The fissure studied was 2.2 m deep and 0.7 m wide at its deepest part, which results in a width/depth ratio of 0.1 and is consistent with the young age of the fissure. Traces of an old fissure near the 1990 fissure are indicated by elongated shallow swales and aligned mesquite bushes adjacent and parallel to the new fissure. This suggests

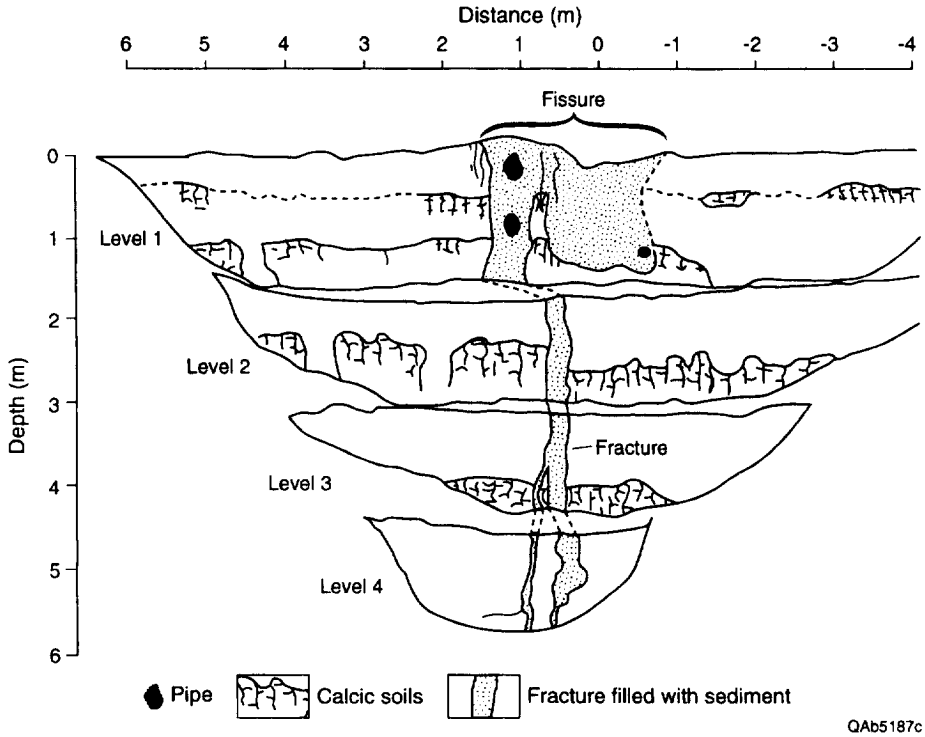

Fig. 3. Cross-section of trench at the Eagle Flat fissure.

that the new fissure is opening where an older fissure existed. Surface collapse of sediment was reported in 1935 also and probably marks the time of a rainfall event that produced erosion and collapse of soils along a pre-existing fracture.

The regional climate is subtropical arid (Larkin and Bomar, 1983). Mean annual precipitation ranges from 280 mm (Hueco Bolson) to 384 mm (Valentine, adjacent to Ryan Flat fissure). Most precipitation falls as local, intense, short-duration convective storms during the summer, when temperature and potential evaporation are highest. Minor winter frontal storms are of longer duration.

2. Methods

Sediment samples were collected for laboratory measurement of physical and chemical parameters from 16 boreholes drilled with an auger rig in and adjacent to four fissures (Fig. 1, Table 1). Borehole names reflect locations relative to the fissure (EF92 0 m is in the fissure, EF92 10 m is 10 m from the fissure). Borehole depths ranged from 8.7 m (RLB 50 m) to 30.6 m (EFF36 10 m). Sediment samples were also collected from a trench excavated in a series of benches (~1.3 m high) that were progressively narrower with depth beneath Eagle Flat fissure (Fig. 3). A grid was placed on the trench face, and samples were collected at ~0.3 m intervals in a 4.2 m wide section at the surface that decreased in width at depth (Fig. 3). A total of 124 samples were collected for water content and chloride analyses. Seven samples were collected for water potential analysis in and adjacent to the fracture fill. The samples were collected immediately after each bench was cleared. Additional material was removed from the trench face with a shovel and knife prior to sampling.

Particle size analyses were conducted on sediment samples by sieving the ≥0.05 mm fraction to determine the percent sand and by conducting hydrometer or pipette analysis of the <0.05 mm fraction to determine the percent silt and clay (Gee and Bauder, 1986). Gravimetric water content was measured by oven

Table 1
Summary of texture, water content, water potential, chloride, chlorine-36, and stable isotope data of samples from boreholes in and adjacent to fissures

Fissure	Borehole	Date drilled	Borehole depth (m)	Gravel (%)	Sand (%)	Silt (%)	Clay (%)	Water content mean ($g\ g^{-1}$)	Unsaturated zone water potential mean (MPa)	Plant water potential mean (MPa)	Chloride mean ($g\ m^{-3}$)	$^{36}Cl/Cl$ mean $\times 10^{15}$	^{3}H mean (TU)	δD_{VSMOW} mean (‰)	$\delta^{18}O_{VSMOW}$ mean (‰)
Hueco Bolson	HBF 0 m	9/7/94	23.90	6	44	23	27	0.09 (1)	−1.9 (3)	−2.7	22 (1)	448	13.5	−53	−7.1
	HBF 10 m	9/4/94	27.00	5	55	19	21	0.06 (2)	−4.9 (4)		48 (2)		25.7		
	HBF 50 m	9/14/94	10.20	9	48	25	17	0.05	−8.8	−4.8	1623	434	35.5	−42	−1.7
Eagle Flat	EHF35 0 m	10/17/92	21.20	2	34	40	24	0.14 (5)	−0.5 (5)	−1.7	N/A				
	EFF36 10 m	10/17/92	30.60	0	30	25	45	0.10	−7.7		5628	373			
	EFF59 10 m	4/18/93	27.50	2	29	26	42	0.11	−6.4		5911				
	EFF88 0 m	5/14/93	13.30	1	36	25	38	0.12 (6)	−1.1 (6)		N/A				
	EFF92 0 m	8/19/94	22.10	0	37	24	39	0.09 (7)	−2.4[a] (7)		1206 (7)	391	18.0	−45	−3.1
	EFF96 10 m	8/31/94	17.00	0	41	22	37	0.09	−8.5		4930		17.1	−43	−1.5
	EFF119 10 m	8/3/95	23.50					0.09	−6.2		4750				
	EFF120 0 m	2/17/96	20.50					0.13 (8)	−0.7 (8)		21 (8)				
	100 m from fissure									−2.0					
Red Light Bolson	RLBF 0 m	8/23/94	16.10	9	36	30	25	0.07	−2.7	−2.3	112	713		−55	−7.1
	RLBF 50 m	8/24/94	8.70	5	41	29	25	0.05	−5.9	−2.0	2268			−43	−2.0
Ryan Flat	RFF 0 m	9/3/94	25.30	3	34	22	41	0.16	−1.4	−1.6	97	575	8.9	−52	−5.4
	RFF 10 m	9/2/94	16.30	1	37	25	37	0.12	−3.8		737	544			
	RFF 50 m	9/1/94	13.30	0	39	23	38	0.14	−3.2	−3.4	437		20.5	−45	−3.0

BDL: below detection limit of 2 $g\ m^{-3}$ in the supernatant.

Calculated mean using samples generally from above the chloride front in the upper (1) 14 m, (2) 12 m, (3) 1 to 12 m, (4) 1 to 11 m, (5) 9.1 m, (6) 5.8 m, (7) 5.9 m, and (8) 7.7 m. Mean chloride concentrations were not calculated for EFF35 0 m and EFF88 0 m because supernatant from many of the samples was below the detection limit.

[a] ≥0.6 m.

drying the sediment samples at 105°C for 24 hr (Gardner, 1986).

Water potential (sum of matric and osmotic potential) was measured in the laboratory using a thermocouple psychrometer with a sample changer (model SC 10A; Decagon Devices Inc., Pullman, WA). The osmotic component of water potential was calculated from pore water chloride concentrations according to the van't Hoff equation (Campbell, 1985Scanlon, 1994). Samples with high water potentials collected from a trench beneath Eagle Flat fissure were analyzed using both the Decagon SC 10A sample changer and the filter paper method (ASTM, 1992). The filter paper was placed in the center of the sediment samples in glass containers and was allowed to equilibrate for 2 weeks. After equilibration, the mass of the filter paper was measured and was related to the matric potential through calibration curves developed by Greacen et al. (1987).

Predawn plant water potentials were measured in and adjacent to the fissures using a portable pressure chamber apparatus (Plant Moisture Stress Inc., Corvallis, OR) by removing at least two randomly chosen stems containing leaves from each plant and immediately measuring their water potential. The stems were wrapped in plastic to minimize sample drying prior to measurement and to prevent sample burning by nitrogen in the pressure chamber. Stems were collected from mesquite plants within and adjacent to fissures except at the Hueco Bolson fissure, where mesquite trees were not found outside the fissure. Creosote bushes were sampled in and adjacent to the Hueco Bolson fissure instead. Plant water potentials were measured periodically for one year. Samples were not collected in March because the plants were defoliated and dormant.

To determine chloride content, double-deionized water was added in a 3:1 ratio to the dried sediment samples that had previously been analyzed for water content. Samples were agitated on a reciprocal shaker table for 4 hr. The supernatant was filtered through 0.45 μm filters. Chloride was then analyzed by ion chromatography or by potentiometric titration, and chloride concentrations in pore water were calculated according to procedures outlined in Mattick et al. (1987). Chloride concentrations are expressed as g Cl m^{-3} pore water (equivalent to mg Cl l^{-1} pore water).

Laboratory preparation of chloride samples for ^{36}Cl analysis followed procedures outlined in Scanlon (1992a). The $^{36}Cl/Cl$ ratios were measured by accelerator mass spectrometry at Lawrence Livermore National Laboratory. Water for tritium analysis was extracted from sediment samples by azeotropic distillation with toluene (Allison et al., 1985). Tritium was analyzed by the University of Arizona Tritium Laboratory using enrichment factors that ranged from 2 to 9 depending on the amount of water available. The detection limit for enriched tritium analyses was 0.7 TU and the standard errors were $\leq$1.4 TU. Stable isotope analyses of oxygen and hydrogen were conducted by the Desert Research Institute according to procedures outlined in Ingraham and Shadel (1992).

Apparent electrical conductivity of the subsurface was measured with an EM31 meter (Geonics Inc., Mississauga, Canada) along transects perpendicular to the trend of the fissures for distances of up to 100 m on either side. The theoretical basis for these measurements is described in McNeill (1992). The intercoil spacing in the EM31 is 3.7 m and the exploration depth is ~3.0 m when the instrument is operated in the horizontal dipole mode and ~6 m when the instrument is operated in the vertical dipole mode.

3. Results

All results are tabulated in Scanlon et al. (1997). Selected profiles are described in the following sections.

3.1. Texture and water content

The texture of the sediments that host the fissures is variable (Table 1). Sediment texture in and adjacent to the Hueco Bolson and Red Light Bolson fissures is much coarser grained than that in and adjacent to the Eagle Flat and Ryan Flat fissures. This reflects the regional geologic setting of these fissures. Sediment samples beneath and adjacent to the Hueco Bolson fissure have mean sand contents that range from 44 to 55% in the different profiles (Table 1). Textures in the Red Light Bolson fissure are generally coarse grained (mean sand content 36 to 41%). In contrast,

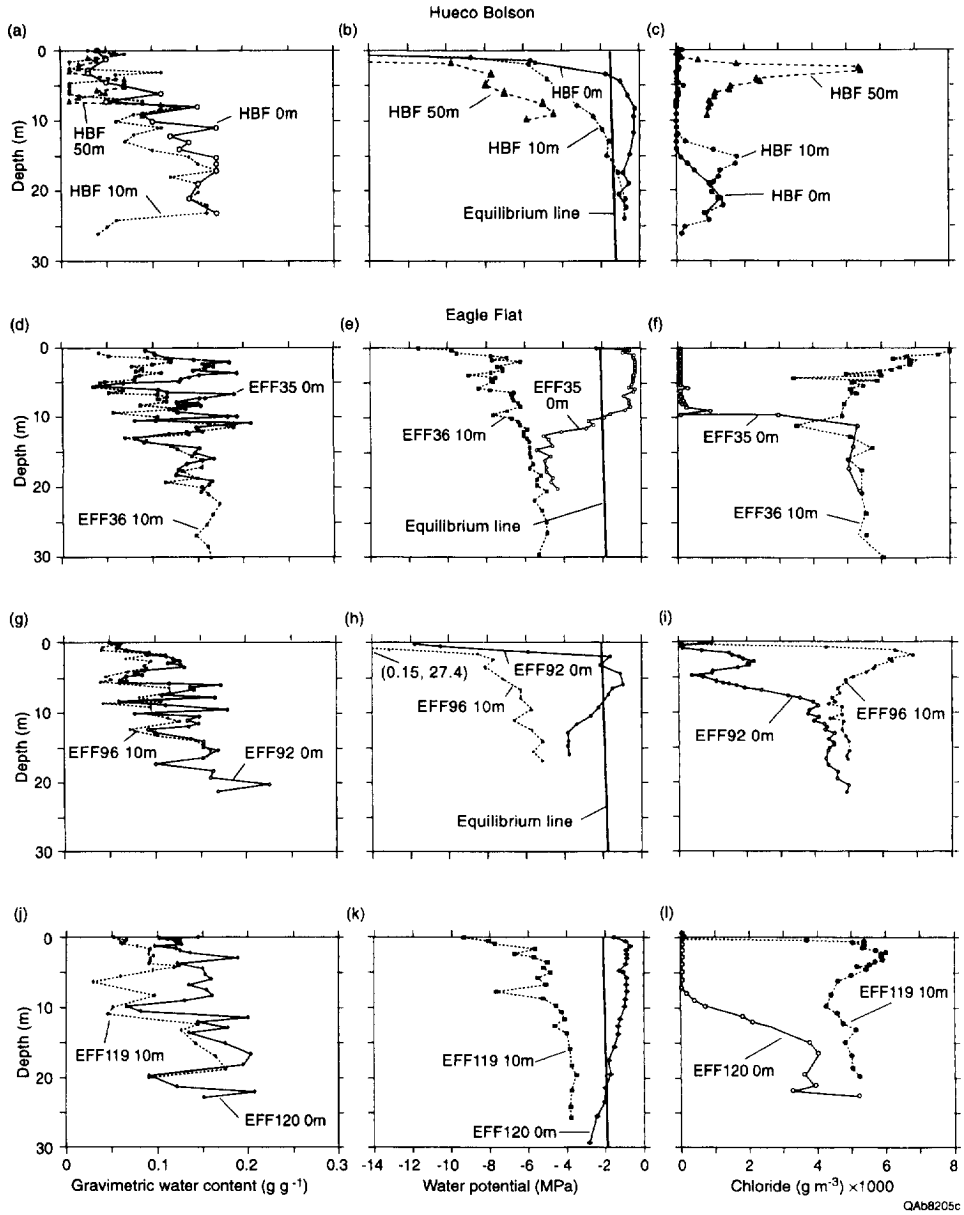

Fig. 4. Profiles of water content, water potential, and chloride concentrations in and adjacent to Hueco Bolson and Eagle Flat fissures.

textures beneath Eagle Flat fissure are predominantly silt (mean: 22 to 40%) or clay (mean: 24 to 45%) and those beneath Ryan Flat fissure are predominantly clay (mean: 37 to 41%) with local zones of gravelly material.

The boreholes were drilled at different times (Table 1), which may affect interborehole comparisons. Water content in all profiles in Eagle Flat fissure was higher than that in profiles 10 m from the fissure at least in the upper 5 to 10 m (Fig. 4(d, g, j)). These differences in water content cannot be attributed to textural differences and are related to higher water fluxes beneath the fissure. Water content differences were greatest between EFF120 0 m and EFF119 10 m,

Table 2
Water potentials measured with the filter paper method and the Decagon SC10A thermocouple psychrometer on samples taken from trench beneath Eagle Flat fissure

Distance (m) from surface depression	Depth (m)	Location	Water potential (MPa) (filter paper)	Water potential (MPa) (Decagon)
0.6	0.3	adjacent to fracture	−0.02	−0.12
0.3	0.3		−0.02	−0.06
0	0.2	in fracture fill	−0.01	0.03
0	0.6		−0.01	−0.05
0	1		−0.01	0.01
−0.3	0.3	adjacent to fracture	−0.16	−0.18
−0.6	0.3		−0.20	−0.20

which are located in the central portion of the fissure where there is a large gully (Fig. 4(j)). In contrast, there was no systematic variation in water content in profiles beneath and adjacent to the other fissures (Fig. 4(a); Fig. 5(a, d); Table 1). Spatial variations in water content were generally related to variations in sediment texture. Water content was negatively correlated with percent sand and gravel and was positively correlated with percent clay (Scanlon et al., 1997). The lack of variations in water content between profiles in three of the four fissures relative to profiles adjacent to these fissures may be related in part to the sampling time. Boreholes in and adjacent to Hueco Bolson, Red Light Bolson, and Ryan Flat fissures were drilled in 1994, when precipitation was much less than the long-term mean precipitation. Precipitation in 1994 was only 33% of the long-term mean (280 mm) in the Hueco Bolson, 44% of the long-term mean (320 mm) in Sierra Blanca (adjacent to Eagle Flat fissure), and 40% of the long-term mean (384 mm) in Valentine (adjacent to Ryan Flat fissure).

3.2. Unsaturated zone water potentials

Water potentials in the unsaturated zone were generally higher in profiles beneath the fissures than in profiles adjacent to the fissures in the upper 6 to 15 m (Fig. 4(b, e, h, k); Fig. 5(b, e); Table 1). Water potentials were as high as −0.2 MPa beneath the Hueco Bolson, Eagle Flat, and Ryan Flat fissures. These water potentials may not be highly accurate because of the standard error of the laboratory-measured water potentials with the Decagon SC 10A thermocouple psychrometer in this range (~ ± 0.06 MPa). Water potentials measured with the filter paper method for samples collected in the trench beneath Eagle Flat fissure agreed well with those measured with the Decagon thermocouple psychrometer for the range between −0.20 and −0.16 MPa; however, the agreement was poor in the wetter range where some of the water potentials measured by the Decagon thermocouple psychrometer were positive (Table 2). Water potentials were higher in the fracture fill material (−0.01 MPa) than in the adjacent sediments (−0.16 to −0.20 MPa). The Eagle Flat fissure differs from the other fissures in that water potentials decreased below the zone of high water potentials (Fig. 4(e, h, k)), whereas in all the other profiles water potentials remained high at depth (Fig. 4(b); Fig. 5(b, e)). This reduction in water potential at depth in the Eagle Flat fissure marks the wetting front and is most clearly seen in EFF35 0 m (Fig. 4(e)) and is more diffuse in the other profiles beneath Eagle Flat fissure (Fig. 4(h, k)). In profile EFF35 0 m, water potentials decreased from −0.8 MPa at 9.1 m to −5.0 MPa at 12.8 m depth. Below 13 m, water potentials in EFF35 0 m were similar to those in the profile 10 m from the fissure (EFF36 10 m). Water potentials in the other profiles beneath Eagle Flat fissure (EFF88 0 m, Scanlon et al., 1997; EFF92 0 m; and EFF120 0 m) were generally lower than those in EFF35 0 m.

Below the shallow subsurface, water potential gradients were generally close to zero beneath the fissures, indicating downward flow (Fig. 4(b, e, h, k);

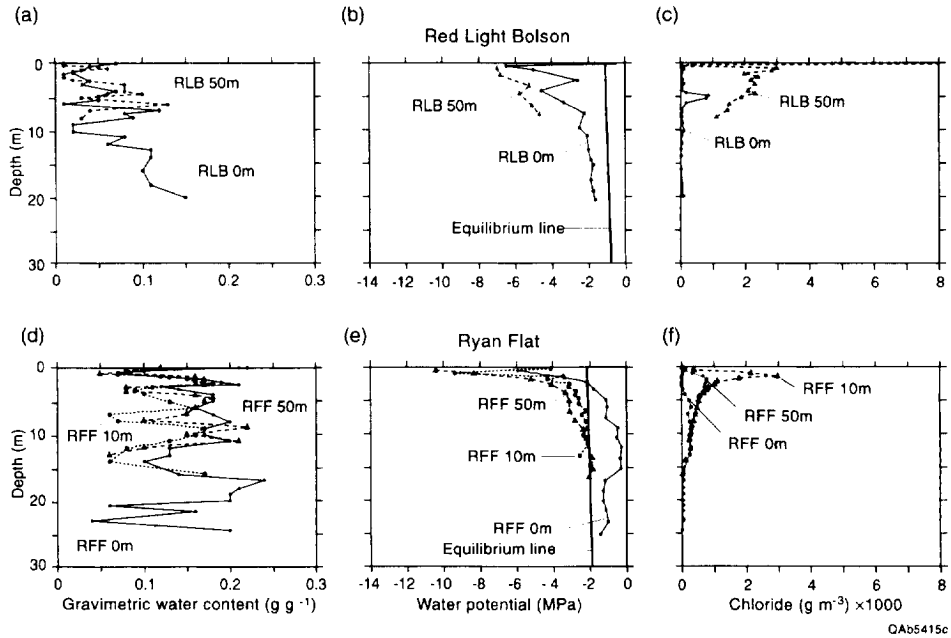

Fig. 5. Profiles of water content, water potential, and chloride concentrations in and adjacent to Red Light Bolson and Ryan Flat fissures.

Fig. 5(e)). A zone of low water potentials in the shallow subsurface in some profiles beneath the fissures indicates near-surface evapotranspiration (Fig. 4(b, h); Fig. 5(e)). Water potentials in profiles adjacent to the fissures were low at the surface (≥ -27.4 MPa) and generally increased with depth, which indicates an upward driving force for water movement (Fig. 4(b, e, k); Fig. 5(b, e)). These profiles plot to the left of the static equilibrium line (matric potential = gravitational potential; no flow line), which further indicates upward flow under steady flow conditions. The low precipitation in 1994, when many of the boreholes were drilled, may have affected the difference in water potentials between profiles beneath and adjacent to fissures.

3.3. Plant water potential

Predawn water potentials in plants were significantly higher in Hueco Bolson ($\alpha = 0.05$), Eagle Flat ($\alpha = 0.06$), and Ryan Flat ($\alpha = 0.05$) fissures than adjacent to these fissures (Fig. 6). The difference in predawn plant water potentials was most obvious in Ryan Flat fissure, which is a very active fissure (Fig. 6(c)). The average water potential in plants at this fissure was −1.6 MPa, whereas that in plants adjacent to the fissure was −3.4 MPa. Mean plant water potentials ranged from −2.7 MPa in the Hueco Bolson fissure to −4.8 MPa 50 m from the fissure (Table 1). The difference in mean plant water potentials between Eagle Flat fissure (−1.7 MPa) and 50 m from the fissure (−2.0 MPa) was much less than that in the other settings. There was no systematic difference in predawn plant water potentials in Red Light Bolson fissure relative to the adjacent area (Scanlon et al., 1997). The monitoring interval was not sufficient to evaluate seasonal or shorter-term variations in plant water potentials.

3.4. Environmental tracers

3.4.1. Meteoric chloride

In general, chloride concentrations were lower in profiles beneath fissures than in profiles adjacent to fissures (Fig. 4(c, f, i, l); Fig. 5(c, f); Table 1). Previous studies of the Hueco Bolson fissure showed low chloride concentrations (≤ 110 g m^{-3}) in the upper 10 m in the profile immediately beneath the fissure and in profiles at 3 and 6 m from the fissure (Scanlon, 1992b). In this study, profiles beneath the

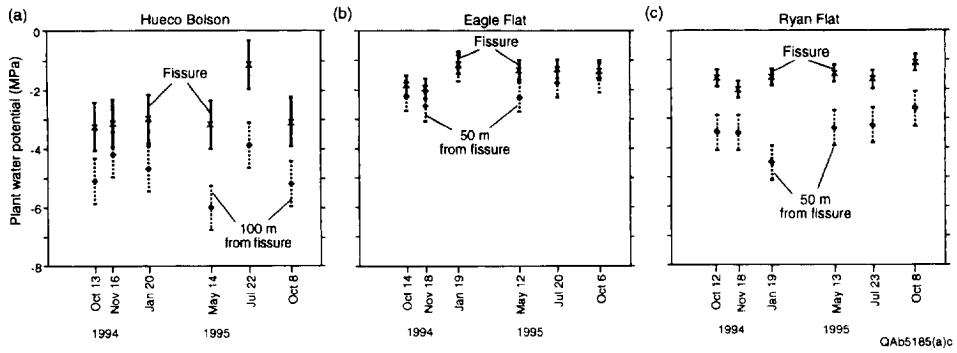

Fig. 6. Comparison of predawn plant water potentials measured in and adjacent to fissures.

Hueco Bolson fissure and 10 m from the fissure had low chloride concentrations (mean 20 g m^{-3}, upper 14 m, beneath fissure; mean 48 g m^{-3}, upper 12 m, 10 m from fissure), whereas chloride concentrations in the profile 50 m from the fissure were high (mean 1623 g m^{-3}, maximum Cl, 5437 g m^{-3}, 3.1 m depth, Fig. 4(c)). Chloride concentrations beneath the fissure increased from 2.5 g m^{-3} (14.1 m depth) to 1300 g m^{-3} (21.1 m depth) that probably marks the extent of flushing. The profile 10 m from the Hueco Bolson fissure also had a chloride front that is sharper than that beneath the fissure and is also shallower (2.9 g m^{-3} at 11.0 m to 1792 g m^{-3} at 15.2 m).

The zone of low chloride concentrations is restricted to beneath the Eagle Flat fissure, whereas the profile 10 m from the fissure has high chloride concentrations (Fig. 4(f, i, l)). Chloride concentrations were low ($\leq$196 g m^{-3}) in the upper 9 m of the profile EFF35 0 m and increased sharply to 5205 g m^{-3} within a 2 m depth interval (Fig. 4(f)). The solute front in EFF120 0 m was much more diffuse, the chloride concentrations increased from $<$158 g m^{-3} in the upper 8.3 m to 4008 g m^{-3} at 16.7 m depth (Fig. 4(l)). The vertical extent of chloride leaching and the degree of leaching are similar in EFF35 and EFF120 (Fig. 4(f, l)), but both were much less in EFF88 (Scanlon et al., 1997) and EFF92 (Fig. 4(i)). Chloride concentrations at depth beneath the Eagle Flat fissure were similar to those in the profiles 10 m from the fissure (Fig. 4(f, i, l)). Chloride profiles adjacent to Eagle Flat fissure had highest concentrations at or near the surface and generally decreased with depth. The solute front in EFF35 0 m correlates with a slight reduction in chloride in the profile 10 m

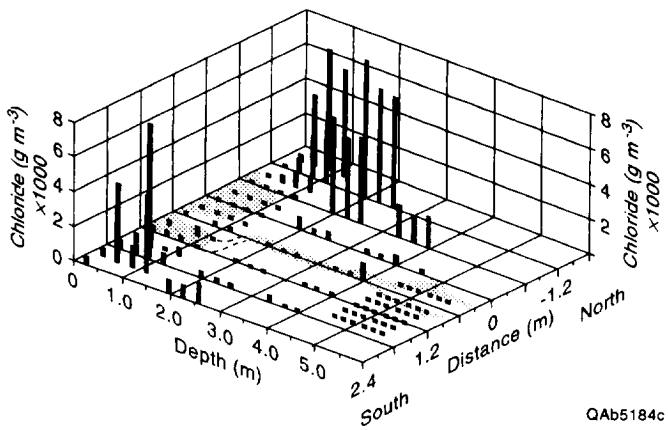

Fig. 7. Spatial variability in chloride concentrations in a trench beneath Eagle Flat fissure. The dashed section marks the location of the fissure and underlying sediment filled fracture.

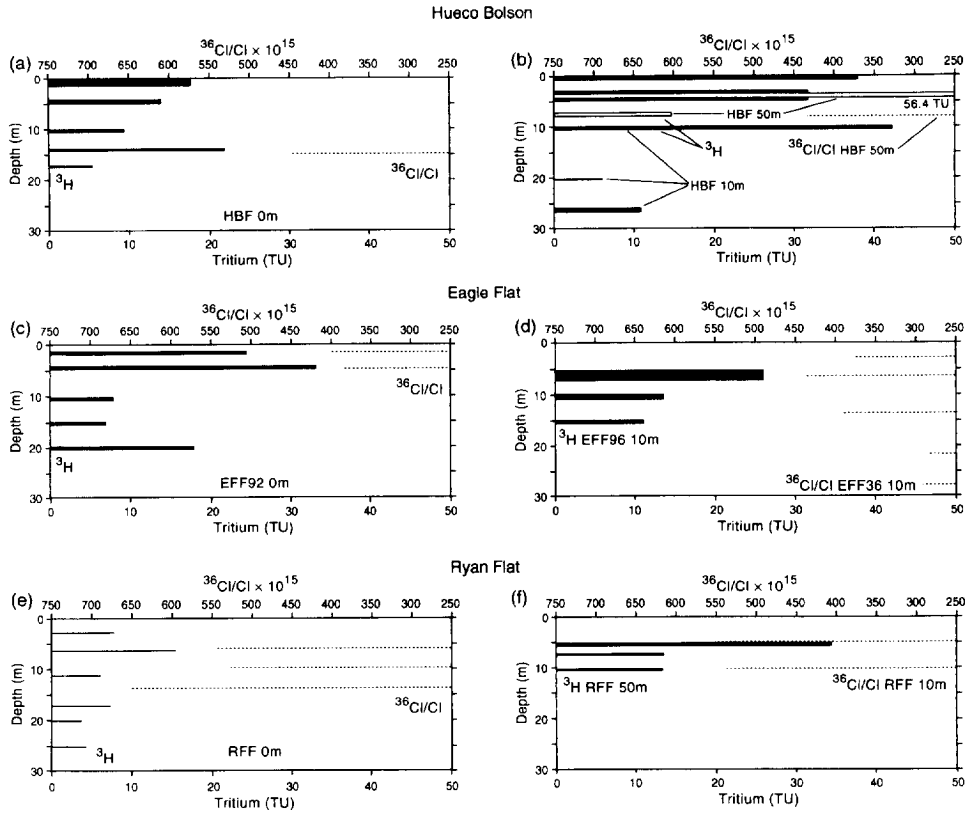

Fig. 8. Variations in ^{3}H and ^{36}Cl/Cl in profiles in and adjacent to fissures.

distant from 4746 g m^{-3} at 9.9 m depth to 3405 g m^{-3} at 11.3 m depth, which may reflect lateral flow. Sharp changes in chloride concentrations are also found in EFF59 10 m (reduction from 5510 g m^{-3} at 14.2 m depth to 3286 g m^{-3} at 15.8 m depth and increase to 8804 g m^{-3} at 17.4 m depth, Scanlon et al., 1997).

Detailed sampling in a trench in Eagle Flat fissure (Fig. 3, Fig. 7) showed that the horizontal extent of chloride flushing was much more restricted than the 10 m extent that was estimated from the borehole data. The sampling grid was centered on the surface expression of the fissure; however, the subsurface fracture was offset to the south of the surface fissure by ~0.6 m. High chloride concentrations were found at a distance of ~1.2 m north of the underlying fracture at depths of 2 to 3 m and generally at distances ≥1.8 m south of the surface expression of the fracture. The shape of the trench precluded sampling along a uniform grid.

Chloride concentrations in the profile beneath Red Light Bolson fissure were low throughout (≤97 g m^{-3}) with the exception of a local higher zone (151 to 844 g m^{-3}) from 4.5 to 6.0 m depth (Fig. 5(c)). The chloride profile 50 m from the fissure had high chloride concentrations that ranged from 2991 g m^{-3} at 0.76 m depth to 1141 g m^{-3} at 8.2 m depth. Chloride concentrations were fairly low (≤292 g m^{-3}) throughout the profile in Ryan Flat fissure and increased gradually away from the fissure (Fig. 5(f)). Maximum concentrations were 2980 g m^{-3} at 1.3 m depth in the profile 10 m from the fissure and 757 g m^{-3} at 1.7 m depth in the profile 50 m from the fissure. At depths ≥10 m all three profiles had similar chloride concentrations (8 to 297 g m^{-3}).

3.4.2. Isotopes

It was difficult to collect sufficient chloride for ^{36}Cl analysis beneath fissures. Where sufficient chloride

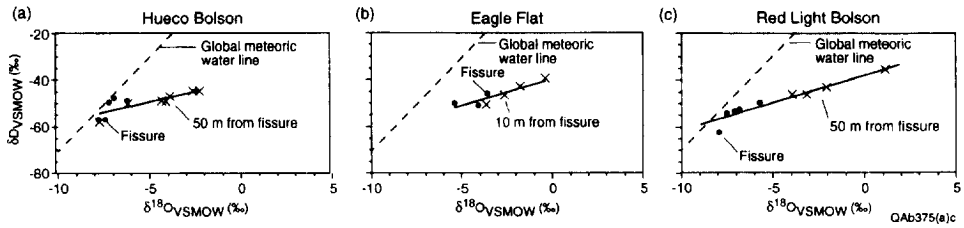

Fig. 9. Stable isotopes of oxygen and hydrogen in and adjacent to fissures.

was available, $^{36}Cl/Cl$ ratios were low (383×10^{-15} at 4.7 m depth in EFF 92 (Fig. 8(c)) to 713×10^{-15} at 4.7 m depth in RLB 0 m) and do not indicate significant contribution from the bomb pulse. Previous studies in an ephemeral stream setting at the Hueco Bolson study area included analysis of the distribution of bomb pulse ^{36}Cl and showed that the $^{36}Cl/Cl$ ratios typical of the bomb pulse reached a maximum value of 6560×10^{-15} (Scanlon, 1992a) and prebomb $^{36}Cl/Cl$ ratios were $\sim 460 \times 10^{-15}$.

Tritium concentrations were high in all profiles analyzed for tritium beneath and adjacent to fissures (Fig. 8). There was no systematic variation in tritium concentrations with depth. Tritium concentrations were high in profiles beneath the Eagle Flat fissure and beneath and 10 m from the Hueco Bolson fissure (Fig. 8(a, b)), which is consistent with chloride being flushed out in these profiles also. Tritium concentrations were also high in the profile 10 m from the Eagle Flat fissure (Fig. 8(d)), 50 m from the Hueco Bolson fissure (Fig. 8(b)) and 50 m from the Ryan Flat fissure (Fig. 8(f)) although chloride concentrations were high in these profiles also (Fig. 4(c,i) and Fig. 5(f)). High tritium concentrations were found beneath the chloride solute fronts in the Hueco Bolson and Eagle Flat fissure profiles (Fig. 8(a, b, c, d)).

Stable isotopes of oxygen and hydrogen were less enriched in profiles in fissures relative to those adjacent to fissures (Fig. 9). This suggests less evaporation of the water in sediments beneath fissures than in sediments adjacent to fissures. In HBF 50 m, EFF92 0 m, and EFF96 10 m profiles the surface samples were much more enriched than deeper samples. Statistical tests that omitted the surface samples showed that differences in $\delta^{18}O$ between sediments beneath fissures relative to those adjacent to fissures were significant at $\alpha = 0.05$.

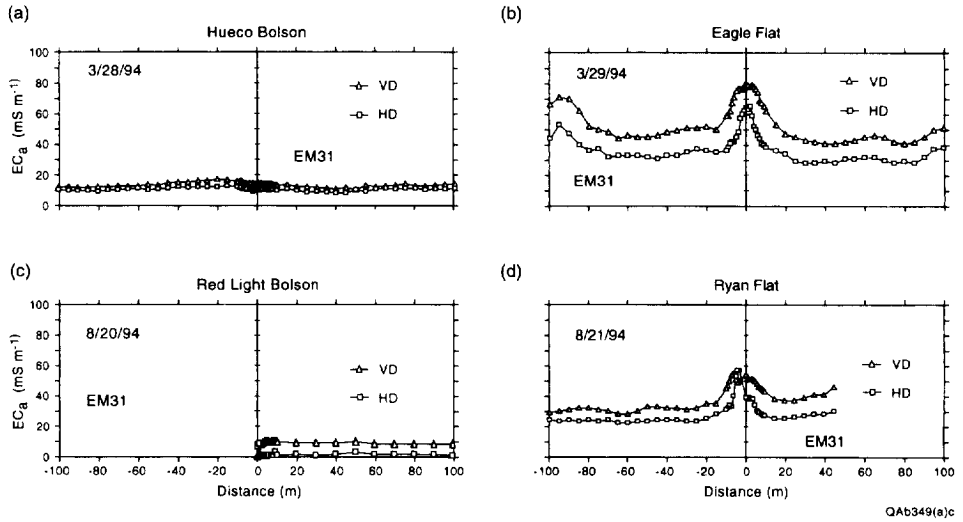

Fig. 10. Electromagnetic transects across fissures.

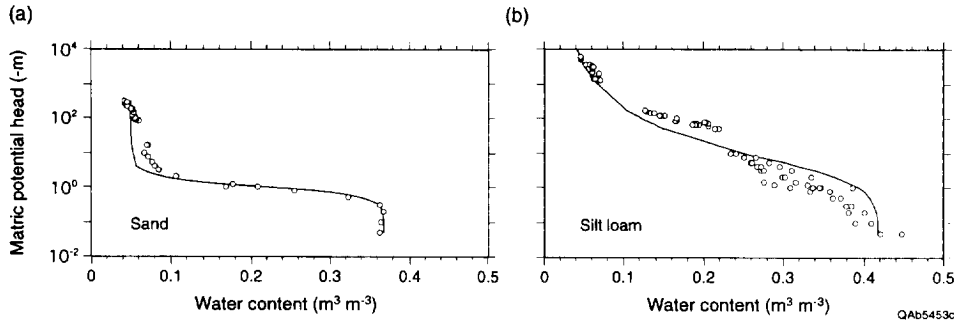

Fig. 11. Water retention curves for sediment samples from the Eagle Flat study area.

3.4.3. Electromagnetic induction

Three different fissures, Eagle Flat fissure (Fig. 10(b)), a section of Red Light Bolson fissure (Scanlon et al., 1997), and Ryan Flat fissure (Fig. 10(d)), showed higher apparent electrical conductivities in the vicinity of the fissure relative to the area adjacent to the fissure. In each case, apparent conductivities increased by a factor of ~2 in the vicinity of the fissure in both the vertical and horizontal dipole modes. The other fissures, Hueco Bolson fissure (Fig. 10(a)) and another section of Red Light Bolson fissure (Fig. 10(c)), showed negligible variation in apparent conductivity in the vicinity of the fissure. This section of the Red Light Bolson fissure (Fig. 10(c)) differs from the other (Scanlon et al., 1997) in that the width/depth ratio of the fissure is much greater and probably represents a less active section of the fissure. The previously discussed borehole data are from the older section of the fissure. Two transects were conducted across Eagle Flat fissure, one where there was a gully at the surface to mark the location of the fissure (Fig. 10(b)) and a second parallel to the first but where there was no gully present (Scanlon et al., 1997). Apparent conductivity along the transect where there was no gully was similar to that along the transect where the gully was present (Fig. 10(b)) and indicates that this technique may be suitable for mapping increased subsurface water flux prior to development of surface collapse features associated with fissures. Apparent conductivities measured with the EM31 meter in the vertical dipole mode were higher than conductivities measured in the horizontal dipole mode in the Eagle Flat and Ryan Flat transects (Fig. 10(b,d)). These data indicate that apparent conductivities increased with depth. The two transects (VD and HD) generally parallel each other.

The apparent electrical conductivity of the subsurface is directly proportional to the conductivity of the pore water, to the water content, and to the solid phase conductance (Rhoades et al., 1976, 1989). The solid phase conductance is primarily determined by the clay content and the cation exchange capacity of these clays. Higher values of apparent conductivity across some fissures indicate that variations in water content rather than chloride content control differences in apparent conductivities across these fissures. If chloride content were controlling apparent conductivities, values should be reduced across fissures because chloride is flushed out. Because measured apparent conductivity is controlled mostly by variations in water content, this is not a very useful method for detecting higher water fluxes beneath fissures because water content varies also with texture and increased water content is not highly characteristic of sediments beneath fissures. Low chloride content provides a more distinctive signature of high water flux in sediments beneath fissures. The lack of variation in apparent conductivity in some fissures (Hueco Bolson and a section of Red Light Bolson; Fig. 10(a, c)) is attributed to water contents being too low to conduct electricity. This is supported by comparisons of downhole electrical conductivity measurements with an EM39 instrument and measured water content for the Hueco Bolson fissure, which shows that the threshold water content is approximately 0.07 g g^{-1} (Paine et al., 1997). The EM induction measurements were done in 1994, when precipitation was much lower than the

long-term mean annual precipitation. Differences in apparent conductivities between sediments beneath and adjacent to fissures may be much greater after long wet periods.

4. Discussion

4.1. Unsaturated flow in sediments beneath fissures

The physical and chemical data are consistent and show that subsurface water fluxes are higher in sediments beneath fissures than in sediments adjacent to fissures. Higher water potentials, lower chloride concentrations, high tritium levels, and less enriched stable isotopes in profiles in fissures relative to profiles adjacent to fissures indicate increased water flux beneath the fissures. A variety of fissures were examined in this study. Physical and chemical parameters vary within short intervals along the Eagle Flat fissure which indicates that there is almost as much variability along individual fissures as there is between fissures. The various profiles in Eagle Flat fissure indicate different degrees of flushing of the pore water chloride that may be related to small-scale topographic changes along the fissure. Low water potentials and high chloride concentrations typical of profiles adjacent to fissures indicate very low water fluxes and are described in Scanlon (1991, 1994).

4.2. Preferential flow

Because surface fissures intercept drainage, water ponds on these features and focuses subsurface flow in the shallow zone. Although some researchers refer to *focused flow* as a macroscopic-scale preferential flow (Gee and Hillel, 1988), most workers restrict the term *preferential flow* to flow along macropores and/or unstable flow. Previous tracer experiments conducted on fissures indicate preferential flow in fracture-fill material (Scanlon, 1992b). High tritium concentrations found throughout the sampled fissure profiles may simply reflect enhanced water flux associated with ponding in the fissures. Penetration of ^{3}H below chloride fronts in the Hueco Bolson and Eagle Flat fissures may reflect preferential flow of water or may reflect the difference between vapor transport of tritiated water relative to liquid transport of chloride. If preferential transport of water containing tritium and chloride (~10%) occurs ahead of the main solute front and this water mixes with the stored water ahead of the main solute front, the resultant tritium and chloride concentrations below the solute front can be estimated using mixing calculations according to the following:

$$C_{mix} = V_p C_p + V_m C_m \quad (1)$$

where C_{mix}, C_p, and C_m are concentrations of tritium or chloride in the mixture, preferentially moving water, and matrix water, respectively; V_p and V_m are the fractional volumes of preferentially moving water and matrix water, respectively, and sum to 1. Mixing 10% water that has bomb pulse tritium (estimated 100 TU) with 90% matrix water stored ahead of the main solute front that has negligible tritium (estimated ~0.01 TU) results in 10 TU in the mixture. Mixing 10% low chloride water (~10 g m^{-3}) that is flowing preferentially ahead of the chloride front with 90% of the in situ high chloride (~5500 g m^{-3}) water ahead of the front results in a concentration of 4951 g m^{-3} in the mixture. The above simple example shows how the tritium levels in water may be greatly affected by preferential flow of bomb pulse water, whereas the chloride concentrations of the pore water should be negligibly affected by preferential flow because the chloride signature of preferentially flowing water is masked by the high chloride concentrations of the pore water ahead of the solute front. Lateral flow as suggested by dilution of chloride in the EFF36 profile 10 m from the fissure may account in part for the tritium levels in the profile 10 m from the fissure.

Vapor transport may also account for deeper penetration of tritium relative to chloride. Previous studies that compared the relative penetration depths of ^{36}Cl and ^{3}H attributed deeper penetration of ^{3}H than ^{36}Cl to vapor transport as a result of thermal vapor diffusion; however, these studies were restricted to the upper meter of the unsaturated zone where temperature gradients are steep (Phillips et al., 1988; Scanlon and Milly, 1994). Tritium is deeper beneath the fissures (≤26 m depth), and temperature gradients are negligible at these depths. Analysis of steady state diffusion of tritium with a concentration of 100 TU at the upper boundary decays to a value of 0.37 times the bounding value at a depth of 0.3 m (Appendix A).

This analysis indicates that vapor diffusion alone cannot account for the much deeper penetration of tritium relative to chloride beneath the fissures. Smiles et al. (1995) also showed that diffusion of tritium in the vapor phase is limited by equilibration between the liquid and gas phases because the concentration of tritium is five orders of magnitude less in the vapor phase than in the liquid phase, reflecting the different densities of water molecules in the two phases. The liquid phase, therefore, acts as a large sink for tritium. Smiles et al. (1995) suggest that barometric pumping should have a negligible effect on tritium concentrations in the unsaturated zone because of the low concentrations of tritium in the vapor phase and rapid equilibration with the liquid phase. High tritium values (e.g., 1100 TU at 24 m depth, ≤162 TU at 109 m depth) have been found adjacent to the Beatty site, Nevada, that cannot readily be explained by liquid or combined liquid and vapor transport (Prudic and Striegl, 1995; Striegl et al., 1996). Until we have a better understanding of vapor transport of tritiated water we cannot assess the significance of the presence of tritium with respect to preferential flow.

Preferential flow is indicated by partial flushing of chloride and moderately high chloride concentrations in some profiles (EFF88 0 m and EFF92 0 m) beneath Eagle Flat fissure. In contrast, very low chloride concentrations in EFF35 0 m and EFF120 0 m indicate that chloride was almost completely flushed out. The water potential and chloride fronts in EFF35 0 m in Eagle Flat fissure are very sharp and suggest that water may be flowing like a piston. Previous studies have used the relative positions of water potential and chloride fronts to evaluate piston-like flow (Jolly et al., 1989) and showed that the ratio of the velocities of solute and wetting fronts (R) based on one-dimensional analytical solutions (Warrick et al., 1971) is:

$$R = \frac{\theta_{wet} - \theta_{dry}}{\theta_{wet}} \quad (2)$$

where θ_{wet} is the water content in the wetted portion of the profile and θ_{dry} is the initial water content ahead of the wetting front. The above analysis indicates that under piston-like flow conditions the solute front should lag behind the wetting front by an amount equal to the amount of initial water in the profile prior to infiltration. If we assume that the water content in the profile 10 m from the Eagle Flat fissure (EFF36 10 m) represents the initial water content (θ_{dry}, 0.11 $m^3 m^{-3}$) in the upper 10 m of the profile beneath the fissure (EFF35 0 m), and that θ_{wet} is the mean water content in the upper 10 m of EFF35 0 m (0.20 $m^3 m^{-3}$), then the velocity of the solute front should be ~0.5 times that of the wetting front. This difference in velocities should result in much greater separation in the water potential and chloride fronts than is found (Fig. 4(e, f)). An alternative explanation of the sharp chloride front beneath the Eagle Flat fissure may be provided by the natural capillary barriers created by the distinct layering of sediments in the profile. The depth of the solute front corresponds approximately to an increase in sand content from 13 to 65%. In the presence of natural capillary barriers, water would accumulate on top of the coarse textured layer until the water potential increased sufficiently to overcome the water entry pressure of the underlying coarse layer. While water is accumulating on the coarse layer, the separation between the wetting and solute fronts would decrease. In addition, the above analysis of the relative velocities of wetting and solute fronts was based on one-dimensional flow; however, water flow beneath Eagle Flat fissure may be two-dimensional. Reductions in chloride in EFF36 10 m at depth may be related to lateral flow along a capillary barrier. Low chloride concentrations at approximately 5 m depth in EFF88 0 m and EFF92 0 m may also reflect lateral flow along a capillary barrier because a sand layer is found at this depth. Therefore, natural capillary barriers may retard flow and sharpen fronts; however, this does not mean that water movement is piston-like above the capillary barrier.

4.3. Water flux estimates

Chloride profiles in sediments beneath fissures cannot be used directly to estimate water fluxes because the chloride in the profiles probably represents residual chloride that reflects incomplete flushing of the chloride and does not therefore represent the current flux through the sediments. This is most apparent in profiles EFF88 0 m and EFF92 0 m. In contrast, the chloride in profiles EFF35 0 m and EFF120 0 m is much lower and represents more complete flushing.

If the time when fluxes increased in sediments beneath fissures were known, one could estimate the

water fluxes from the depth of the solute fronts found in Eagle Flat and Hueco Bolson fissures. The vegetation linear associated with Eagle Flat fissure is clearly visible in aerial photographs taken in 1957 (Jackson et al., 1993); however, the fissure may have been active for a much longer time. Use of a minimum age for the initiation of the fissure will result in a maximum water velocity for unsaturated flow in sediments beneath fissures. If we assume that Eagle Flat fissure has been present for 50 yr, and we approximate the location of the chloride front to be 9 m, then the resultant water velocity would be 180 mm yr^{-1}. The resultant water flux would be 36 mm yr^{-1}, based on an average volumetric water content of 0.2 $m^3 m^{-3}$ (θ_g, 0.14 g g^{-1}; bulk density, 1400 kg m^{-3}). This flux may be much greater than the actual water flux if the age of the fissure is much older.

A similar analysis was done for the Hueco Bolson fissure, on the assumption that this fissure has been present for 50 yr. The midpoint of the chloride front is taken to be 17 m beneath the fissure and 14 m in the profile 10 m from the fissure. This results in velocities of 340 mm yr^{-1} beneath the fissure and 280 mm yr^{-1} 10 m from the fissure. The average volumetric water content is 0.14 $m^3 m^{-3}$ beneath the fissure and 0.10 $m^3 m^{-3}$ in the profile adjacent to the fissure (assuming a bulk density of 1400 kg m^{-3}) and results in a water flux of 48 mm yr^{-1} beneath the fissure and 28 mm yr^{-1} adjacent to the fissure. A portion of the water is flowing faster than represented by the chloride front, as indicated by the presence of bomb pulse tritium down to 26 m depth in the profile 10 m from the Hueco Bolson fissure. However, the percent of water flowing below the solute front cannot be determined with available data. Water velocities estimated from the tritium data range from 550 mm yr^{-1} directly beneath the fissure (tritium down to 17 m depth) to 840 mm yr^{-1} 10 m from the fissure. This assumes that the tritium represents peak fallout in 1963 and uses the period between peak fallout and sampling (1994) to estimate the velocity. Because the percent of water involved in the tritium transport cannot be estimated, water fluxes cannot be obtained from the tritium data.

4.4. Comparison of different techniques to evaluate flow in areas containing fissures

Multiple independent lines of evidence were used to evaluate subsurface water fluxes in sediments beneath fissures. The effectiveness of various techniques in delineating unsaturated flow varied. Although water content in sediments is readily measured, only the Eagle Flat area had substantially higher water content beneath the fissure relative to the profile 10 m from the fissure. In the other fissures, variations in water content with texture masked any small differences in water content that may have occurred between fissure and nonfissure settings. Unsaturated zone water potential is a much more sensitive indicator of higher water flux beneath fissures than water content. In many profiles the water potentials near the surface in the upper 0.5 to 1 m zone were low and probably reflected drying of these sediments. At greater depths, the water potential profiles in the fissures were up to an order of magnitude greater than water potentials in adjacent profiles.

The significance of these water potential differences depends on the water retention functions of the sediments which describe the relationship between water potential and water content. Water retention curves were developed for coarse- and fine-textured sediments from the Eagle Flat study area (Fig. 11). In coarse-textured sediments as found in the Hueco Bolson, the difference from −0.3 MPa beneath the fissure to ~−3 MPa in the profile 10 m from the fissure reflects very little change in water content (≤0.03 $m^3 m^{-3}$) because these points are in the steep section of the water retention curve (Fig. 11(a)). In contrast, the water potential difference from −0.3 MPa in Eagle Flat fissure to −3 MPa in the profile 10 m from the fissure reflects a large change in water content (~0.1 $m^3 m^{-3}$) for silt loam material (Fig. 11(b)) and is consistent with the water content differences between sediments beneath fissures and sediments adjacent to fissures found in the Eagle Flat area. Therefore, the significance of the water potential differences with respect to water flux varies with texture. Large water potential differences in coarse-textured sediments may reflect only slight changes in water flux; therefore, water potential differences are much more sensitive indicators of small changes in water flux than water content.

Although fissures examined in this study commonly have dense vegetation along them that can be seen as vegetation linears on aerial photos, variations in predawn plant water potentials were not very good

indicators of increased water flux in sediments beneath fissures. Clearly, vegetation plays a critical role in removing infiltrated water, as seen in the large temporal variations in water content in Eagle Flat fissure (Scanlon et al., 1997). Differences in predawn plant water potentials were not as great as those in unsaturated zone water potentials between sediments beneath and adjacent to fissures. The contrast in mean plant water potentials between the Hueco Bolson fissure (−2.7 MPa) and 50 m from the fissure (−4.8 MPa) was not as great as the contrast in water potential profiles in the unsaturated zone (Fig. 4(b)). Creosote bushes were sampled in the Hueco Bolson because there were no mesquite trees outside the fissure. Although large roots were found in fracture-fill sediments in trenches dug to 6 m depth in this fissure (Scanlon, 1992b), rooting depths for creosote are generally less than 2 m. Therefore, the plants in the Hueco Bolson area may be sampling the shallow subsurface, which is generally drier than deeper sections of the fissure profile. The lack of information on the sampling depths represented by the plant water potentials makes detailed comparisons of plant and sediment water potentials difficult. Root densities are generally greatest near the surface; therefore, high water potentials at greater depths would not be well represented by the plant data. Differences in mean water potentials for unsaturated zone profiles beneath and adjacent to fissures are not as great as differences in measured water potentials in different depth intervals. Therefore, integrating subsurface water potentials as is done by plants would result in lower differences between sediments beneath and adjacent to fissures.

Chloride concentration in pore water is a reliable indicator of unsaturated flow beneath and adjacent to fissures. All profiles beneath the fissure and in some cases those 10 m from the fissure had low chloride concentrations. Chloride is extremely soluble and is readily flushed out of the sediments; however, chloride in pore water takes a long time (up to thousands of years) to accumulate. Because of the above, the low chloride concentrations in some fissures may be a relict of higher water fluxes in the past and may not represent current conditions. This may be the case in the mature fissures, such as the Red Light Bolson fissure, where low water potentials indicate that the sediments are dry.

Tritium was detected in all samples analyzed for tritium beneath and adjacent to fissures. The maximum vertical or lateral extent of high tritium cannot be determined from these data. As discussed previously, the significance of the high tritium cannot readily be determined. Stable isotopes of oxygen and hydrogen also suggest less enrichment of the water directly beneath the fissures. Differences in the isotope concentrations were not as marked as the differences in water potential and chloride concentrations. The ^{36}Cl data indicated little bomb pulse signature in the profiles beneath the fissures. This may result from dilution of the bomb pulse signature with old residual chloride that was incompletely flushed from the system or may reflect post-1980 water because ^{36}Cl concentrations returned to prebomb levels in the 1980s. Because zones of high flux are associated with low chloride concentrations, it is difficult to collect sufficient chloride for analysis of ^{36}Cl in these zones; therefore, ^{36}Cl is generally not considered a suitable tracer for delineating flow beneath fissures.

Electromagnetic induction is of limited use in defining flow in sediments beneath fissures because the primary control on apparent electrical conductivity variations is water content and water content variations are not very indicative of flow in sediments beneath fissures. In natural interfluvial settings in arid regions, water fluxes and resultant water contents are extremely low and the conductivity corresponding to the water is essentially zero. This corresponds to the threshold water contents of 0.05 $m^3 m^{-3}$ for a sand and 0.12 $m^3 m^{-3}$ for a clay determined by Rhoades et al. (1976). Slightly higher water contents beneath Eagle Flat fissure register as higher apparent electrical conductivities.

The sampling data presented in this study represent the results of collection at one time and cannot be used to evaluate temporal variations in flow in sediments beneath fissures. In addition, most of the sampling was done in 1994, which was an unusually dry year in which annual precipitation was ~40% of the long-term mean values. This sample bias may account for the small differences in some of the hydraulic parameters such as water content, water potential, particularly plant water potential, and electrical conductivity between sediments beneath and adjacent to fissures, but should not affect differences in environmental

tracer distributions such as chloride and tritium because these tracers represent long-term net water fluxes. Considering these factors, sampling should be conducted after long wet periods to maximize differences in hydraulic parameters between sediments beneath and adjacent to fissures.

5. Conclusions

Higher water potentials and lower chloride concentrations in sediments beneath fissures relative to sediments adjacent to fissures indicate higher water fluxes beneath fissures. The lateral extent of high water flux ranged from 1 to >10 m from fissures but was less than 50 m from the fissures. The vertical extent of high water flux was restricted to 10 to 20 m depth, as indicated by steep water potential and chloride fronts in two of the four fissures studied. Water flux estimates based on the position of the chloride front and an assumed age of the Hueco Bolson and Eagle Flat fissures of 50 yr ranged from 28 to 48 mm yr^{-1}. High tritium levels found in profiles beneath and adjacent to fissures cannot readily be explained.

The various techniques used to evaluate flow in sediments beneath fissures differed in their sensitivity to high water fluxes in sediments beneath fissures. Water potential and chloride concentrations were the most sensitive indicators of high water flux. The lower variations in predawn plant water potentials relative to unsaturated zone water potentials between sediments beneath and adjacent to fissures are attributed to plant roots concentrating in near-surface sediments that are generally drier and to the averaging of the unsaturated volume sampled by the roots. Of the isotopes analyzed, tritium indicated high water flux, whereas chlorine-36 was generally unsuitable because of the effect of residual chloride in sediments beneath fissures. Deuterium and oxygen-18 were less enriched beneath the fissures than in adjacent profiles; however, differences in the isotope concentrations were not great. Water content was only useful in delineating high water flux in one fissure. Electromagnetic induction generally mapped water content changes and therefore was not a very good indicator of higher water fluxes beneath fissures. Most of the sample collection was conducted in 1994, which was an unusually dry year and may have affected the differences in hydraulic parameters between sediments beneath and adjacent to fissures. Multiple independent lines of evidence are required to obtain a comprehensive understanding of subsurface flow beneath fissures. Multiple profiles drilled in one fissure indicate that variations in hydraulic parameters and tracer distributions vary substantially along the fissure that may be related to the amount of ponding at the surface.

Acknowledgements

This project was funded under the National Low Level Radioactive Waste Disposal Program under Interagency Contract Number DE-AC07-95ID13223. Conversations with Dr. Scott Tyler on tritium diffusion were very helpful. The authors gratefully acknowledge the cooperation of the landowners (Deron Kasparian and El Paso Water Utilities). The assistance of Junnrien Lai in data analysis is appreciated. Word processing was by Susan Lloyd.

Appendix A

The governing equation for tritium diffusion in the gas phase is:

$$\frac{\partial C}{\partial t} = \frac{\partial(\theta_g C_g + \theta_l C_l)}{\partial t} = D_0 \theta_g \tau \frac{\partial^2 C_g}{\partial z^2} - \lambda(\theta_g C_g + \theta_l C_l) \quad \text{(A1)}$$

where C is the mass of tritiated water per unit volume of soil, θ_g is the volumetric gas content, θ_l is the volumetric liquid content, C_g is the gas concentration (pCi m^{-3} air), C_l is the liquid concentration (pCi m^{-3} water), D_0 is the free air vapor diffusion coefficient, λ is the radioactive decay constant for tritium (0.0559 yr^{-1}). Eq. (A1) is reduced to one variable (C_g) by relating the gas concentration to the liquid concentration using the Henry's Law constant ($K_H = 17.5 \times 10^{-6}$ at 293 K).

$$C_g = K_H C_l \quad \text{(A2)}$$

Substituting Eq. (A2) into Eq. (A1) yields:

$$\frac{\partial\left(\theta_g C_g + \frac{\theta_l}{K_H} C_g\right)}{\partial t} = D_0 \theta_g \tau \frac{\partial^2 C_g}{\partial z^2} - \lambda\left(\theta_g C_g + \frac{\theta_l}{K_H} C_g\right) \quad \text{(A3)}$$

$$\frac{\partial C_g}{\partial t} = D^* \frac{\partial^2 C_g}{\partial z^2} - \lambda C_g \quad \text{(A4)}$$

where

$$D^* = \frac{D_0 \theta_g \tau}{\theta_g + \theta_l / K_H}$$

If we assume that the system is at steady state, i.e. $\partial C_g / \partial t = 0$, Eq. (A4) reduces to:

$$D^* \frac{\partial^2 C_g}{\partial z^2} = \lambda C_g \quad \text{(A5)}$$

If we assign a constant concentration at the surface of 100 TU (3.2×10^5 pCi m^{-3}), and an infinitely deep unsaturated zone, i.e.

$$C_g(z=0) = C_0$$

$$\left.\frac{\partial C_g}{\partial z}\right|_{z=\infty} = 0$$

The solution to Eq. (A4) with the above boundary conditions is:

$$\frac{C_g(z)}{C_0} = e^{\left[-\frac{z\sqrt{\lambda}}{\sqrt{D^*}}\right]} \quad \text{(A6)}$$

Typical values for the parameters for the site are $\theta_g \sim 0.3$, and $\theta_l \sim 0.2$. The tortuosity was estimated from Millington and Quirk (1961) to be ~0.25. $D_0 = 810$ m^2 yr^{-1} (Smiles et al., 1995).

$$D^* = \frac{(810 \text{ m}^2 \text{ yr}^{-1})(0.3)(0.25)}{0.3 + 0.2/17.5 \times 10^{-6}} = 0.005 \text{ m}^2 \text{ yr}^{-1} \quad \text{(A7)}$$

The resultant tritium variation with depth is $\frac{C_z}{C_0} = e^{[-z\sqrt{0.0559/0.005}]} = e^{[-z/0.3]}$. The e folding depth for this exponential function is 0.3 m which is the depth at which the concentration at the upper surface reduces to e^{-1} (= 0.37) times the value at the surface. Therefore, a value of 100 TU at the surface will reduce to 37 TU at 0.3 m depth and to 0.9 TU at 2 m depth. The results of this exercise show that tritium will not migrate very deeply as a result of vapor diffusion because most of the tritium is in the liquid phase. Vapor diffusion cannot explain the deep penetration of tritium to 26 m depth which is below the solute front in the fissure (~9 m depth) or the migration of tritium to the profile 10 m from the fissure.

References

Allison, G.B., Hughes, M.W., 1978. The use of environmental chloride and tritium to estimate total recharge to an unconfined aquifer, Australian Journal of Soil Research, 16, 181–195.

Allison, G.B., Stone, W.J., Hughes, M.W., 1985. Recharge in karst and dune elements of a semi-arid landscape as indicated by natural isotopes and chloride, Journal of Hydrology, 76, 1–26.

ASTM, 1992. The filter paper method. American Society for Testing Materials, Philadelphia, PA. ASTM D-5298-92.

Baumgardner Jr., R.W., Scanlon, B.R., 1992. Surface fissures in the Hueco Bolson and adjacent basins, West Texas. The University of Texas at Austin, Bureau of Economic Geology, Geological Circular 92-2, p. 40.

Bentley, H.W., Phillips, F.M., Davis, S.N., 1986. ^{36}Cl in the terrestrial environment. In: Fritz, P., Fontes, J.C. (Eds.), Handbook of Environmental Isotope Geochemistry, vol. 2b. Elsevier Science, New York, pp. 422–475.

Boling, J.K., 1986. Earth-fissure movements in south-central Arizona, USA. In: Johnson, A.I., Carbognin, L., Ubertini, L. (Eds.), Land Subsidence, Proceedings of the Third International Symposium on Land Subsidence, Venice, Italy, 1984. International Association of Hydrological Sciences Publication No. 151, pp. 757–766.

Campbell, G.S., 1985. Soil Physics with BASIC: Transport Models for Soil–Plant Systems. Elsevier, New York.

Edmunds, W.M., Walton, N.R.G., 1980. A geochemical and isotopic approach to recharge evaluation in semi-arid zones, past and present. In: Arid zone hydrology, investigations with isotope techniques. IAEA, Vienna, IAEA-AG-158/4, pp. 47–68.

Gardner, W.H., 1986. Water content. In: Klute, A. (Ed.), Methods of Soil Analysis, Part 1, Physical and Mineralogical Methods. American Society of Agronomy, Madison, Wisconsin. Monograph 9, pp. 493–545.

Gee, G.W., Bauder, J.W., 1986. Particle-size analysis. In: Page, A.L. (Ed.), Methods of Soil Analysis, Part 2, Chemical and Mineralogical Methods. American Society of Agronomy, Madison, Wisconsin. pp. 383–410.

Gee, G.W., Hillel, D., 1988. Groundwater recharge in arid regions: Review and critique of estimation methods, Hydrological Processes, 2, 255–266.

Greacen, E.L., Walker, G.R., Cook, P.G., 1987. Evaluation of the filter paper method for measuring soil water suction. In: International Conference on Measurement of Soil and Plant Water Status, Logan, UT, pp. 137–143.

Ingraham, N.L., Shadel, C., 1992. A comparison of toluene distillation and vacuum/heat method for extracting soil water for stable isotopic analysis, Journal of Hydrology, 140, 371–387.

Jackson, M.L.W., Langford, R.P., Whitelaw, M.J., 1993. Basin-fill stratigraphy, Quaternary history, and paleomagnetics of the

Eagle Flat study area, southern Hudspeth County, Texas. The University of Texas at Austin, Bureau of Economic Geology, final contract report prepared for the Texas Low-Level Radioactive Waste Disposal Authority, 137p.

Jolly, I.D., Cook, P.G., Allison, G.B., Hughes, M.W., 1989. Simultaneous water and solute movement through an unsaturated soil following an increase in recharge, Journal of Hydrology, 111, 391–396.

Larkin, T.J., Bomar, G.W., 1983. Climatic Atlas of Texas, Dept. of Water Resources, Austin, TX, Publ. No. LP-192, 151pp.

Larson, M.K., Péwé, T.L., 1986. Origin of land subsidence and earth fissuring, northeast Phoenix, Arizona, Association of Engineering Geologists Bulletin, 23 (2), 139–165.

Mattick, J.L., Duval, T.A., Phillips, F.M., 1987. Quantification of groundwater recharge rates in New Mexico using bomb ^{36}Cl, bomb ^{3}H and chloride as soil-water tracers. Water Resources Research Institute, Las Cruces, NM, Report No. 220.

McNeill, J.D., 1992. Rapid, accurate mapping of soil salinity by electromagnetic ground conductivity meters. In: Advances in Measurement of Soil Physical Properties: Bringing Theory into Practice. Soil Science Society of America, Madison, Wisconsin. Special Publication no. 30, pp. 209–229.

Millington, R.J., Quirk, J.P., 1961. Permeability of porous solids, Trans. Faraday Soc., 57, 1200–1207.

Paine, J.G., Goldsmith, R.S., Scanlon, B.R., 1997. Electrical conductivity and gamma ray response to clay, water and chloride content in fissured sediments, Trans-Pecos, Texas. Idaho National Engineering Laboratory, Report DOE/LL 242.

Phillips, F.M., 1994. Environmental tracers for water movement in desert soils of the American Southwest, Soil Science Society of America Journal, 58, 14–24.

Phillips, F.M., Mattick, J.L., Duval, T.A., 1988. Chlorine 36 and tritium from nuclear weapons fallout as tracers for long-term liquid movement in desert soils, Water Resources Research, 24, 1877–1891.

Prudic, D.E., Striegl, R.G., 1995. Tritium and radioactive carbon (^{14}C) analyses of gas collected from unsaturated sediments next to a low-level radioactive-waste burial site south of Beatty, Nevada, April 1994 and July 1995. U.S. Geological Survey, Reston, Virginia. Open-File Report 95-741, 7p.

Rhoades, J.D., Raats, P.A.C., Prather, R.J., 1976. Effects of liquid-phase electrical conductivity, water content, and surface conductivity on bulk soil electrical conductivity, Soil Science Society of America Journal, 40, 651–655.

Rhoades, J.D., Manteghi, N.A., Shouse, P.J., Alves, W.J., 1989. Soil electrical conductivity and soil salinity, new formulations and calibrations, Soil Science Society of America Journal, 53, 433–439.

Robinson, G.M., Peterson, D.E., 1962. Notes on earth fissures in southern Arizona, U.S. Geological Survey Circular, 466, 7p.

Scanlon, B.R., 1991. Evaluation of moisture flux from chloride data in desert soils, Journal of Hydrology, 128, 137–156.

Scanlon, B.R., 1992a. Evaluation of liquid and vapor water flow in desert soils based on chlorine-36 and tritium tracers in nonisothermal flow simulations, Water Resources Research, 28, 185–197.

Scanlon, B.R., 1992b. Moisture and solute flux along preferred pathways characterized by fissured sediments in desert soils, Journal of Contaminant Hydrology, 10, 19–46.

Scanlon, B.R., 1994. Water and heat fluxes in desert soils: 1, Field studies, Water Resources Research, 30, 709–719.

Scanlon, B.R., Milly, P.C.D., 1994. Water and heat fluxes in desert soils: 2, Numerical simulations, Water Resources Research, 30, 721–733.

Scanlon, B.R., Goldsmith, R.S., Gustavson, T.R., 1997. Evaluation of unsaturated flow in fissured sediments in the Chihuahuan Desert, Texas. Idaho National Engineering Laboratory, Idaho Falls, Idaho. Report DOE/LLW-242.

Schumann, H.H., Cripe, L.S., Laney, R.L., 1986. Land subsidence and earth fissures caused by groundwater depletion in southern Arizona, USA. In: Johnson, A.I., Carbognin, L., Ubertini, L. (Eds.), Land Subsidence, Proceedings of the Third International Symposium on Land Subsidence, Venice, Italy, 1984. International Association of Hydrological Sciences, Publication No. 151, pp. 841–851.

Slaff, S., 1989. Patterns of earth-fissure development: Examples from Picacho Basin, Pinal County, Arizona, Arizona Geology, 19 (3), 4–5.

Smiles, D.E., Gardner, W.R., Shulz, R.K., 1995. Diffusion of tritium in arid disposal sites, Water Resources Research, 31, 1483–1488.

Striegl, R.G., Prudic, D.E., Duval, J.S., Healy, R.W., Landa, E.R., Pollock, D.W., Thorstenson, D.C., Weeks, E.P., 1996. Factors affecting tritium and ^{14}Carbon distributions in the unsaturated zone near the low-level radioactive-waste burial site south of Beatty, Nevada. U.S. Geological Survey, Reston, Virginia. Open File Report 96-110, 16p.

Warrick, A.W., Biggar, J.W., Nielsen, D.R., 1971. Simultaneous solute and water transfer for an unsaturated soil. Water Resources Research, 7, 1216–1225.